NANOSYSTEMS:
PHYSICS, CHEMISTRY, MATHEMATICS

Original article

Kononova S.V., et al. *Nanosystems: Phys. Chem. Math.*, 2024, **15** (2), 268–284.
http://nanojournal.ifmo.ru
DOI 10.17586/2220-8054-2024-15-2-268-284

Nanocomposites of aromatic poly(amide-imide) with nanotubular Mg-Fe hydrosilicate

Svetlana V. Kononova[1], Galina K. Lebedeva[1], Valery S. Kozlov[2], Eleonora N. Korytkova[3], Tatyana P. Maslennikova[3], Elena V. Kruchinina[1], Elena N. Vlasova[1], Natalia N. Saprykina[1], Galina N. Gubanova[1], Milana E. Vylegzhanina[1], Vasiliy T. Lebedev[2]

[1]Institute of Macromolecular Compounds Russian Academy of Science, St. Petersburg, Russia

[2]Petersburg Nuclear Physics Institute named by B. P. Konstantinov of National Research Centre "Kurchatov Institute", Gatchina, Russia

[3]Russian Academy of Science, Grebenshchikov Institute of Silicate Chemistry, St. Petersburg, Russia

Corresponding author: Svetlana V. Kononova, svetlanavkononova@gmail.com

ABSTRACT Composite films based on aromatic polyamide imide with carboxyl-containing fragments in repeating units (PAI-Ac) containing hydrosilicate nanotubes $(Mg,Fe)_3Si_2O_5(OH)_4$ are structurally sensitive to the molecular weight of the polymer used. According to Mössbauer spectroscopy data, nanotubes introduced into a polymer matrix generally retain their original structure. When using a polymer with a relatively low molecular weight, composite films are formed that are not stable during the pervaporation of cyclohexane and ethanol. In the case of a high-molecular polymer, the resulting MMM-type membranes are stable during pervaporation. They are more permeable to polar liquids compared to the base polymer and MMMs containing $Mg_3Si_2O_5(OH)_4$ nanotubes. Analysis of the found differences in the properties of the studied nanocomposites with iron-containing nanotubes in the PAI-Ac matrix from similar nanocomposites with magnesium-containing nanotubes leads to the conclusion about the need to study MMMs with iron-containing nanoparticles of a different structure.

KEYWORDS poly(amide-imide), pervaporation, liquid separation, synthesis, hydrosilicate nanotubes, Mössbauer spectroscopy, morphology, composite materials, mixed matrix membranes (MMM), electron microscopy, atomic force microscopy

ACKNOWLEDGEMENTS The work was carried out within State Programs of IMC RAS (Project No. 122012000452-9).

FOR CITATION Kononova S.V., Lebedeva G.K., Kozlov V.S., Korytkova E.N., Maslennikova T.P., Kruchinina E.V., Vlasova E.N., Saprykina N.N., Gubanova G.N., Vylegzhanina M.E., Lebedev V.T. Nanocomposites of aromatic poly(amide-imide) with nanotubular Mg-Fe hydrosilicate. *Nanosystems: Phys. Chem. Math.*, 2024, **15** (2), 268–284.

1. Introduction

The development of inorganic/polymer nanocomposite materials assumes a new importance not only for the experts in the area of polymer mechanics and thermal physics, but for the researchers engaged in membrane technologies whose aim is to design useful materials with valuable mechanical and thermal properties as well as good transport parameters. The works in this field have always been dependent on the availability of nanoparticles and the possibility of synthesis of novel nanosized objects with unique properties. In a number of research papers, it was demonstrated that hybrid systems frequently possessed new characteristics differing from those of the initial compounds [1–3]. These differences are most pronounced upon the formation of filled polymers. The effect is related to the processes of distribution of nanosized inorganic particles in a polymer matrix and is primarily determined by the following factors: (i) the amount and type of reactive groups; (ii) the ability of the initial components to interact with each other; (iii) the presence of "potential ligands" for the selected filler in the polymer structure; (iv) the structure of a filler; (v) the size of filler particles. The rational variation of physico-chemical properties of a polymer by addition of fillers leads to the creation of structural materials with improved characteristics [4–6]. This approach is also used in the development of industrial polymer membranes that should be stable under rigid conditions of the separation process [7]. Composites containing nano-sized inorganic fillers are of particular interest. For example, in a series of publications [8–10], the authors considered the influence of zeolite 4A or carbon molecular sieves introduced into the polyimide matrix on its properties. It has been demonstrated that if the components of a polymer-based composite were well compatible, the ordered nanoporous structure of the inorganic component was responsible for the gas separation efficiency [11, 12]. There are well-known works devoted to the introduction of inorganic (mostly crystalline) additives into a polymeric membrane matrix with the objective of improving its barrier properties with respect to both gases and liquids. This idea was used in the development of composite

membrane materials with decreased gases and liquids permeabilities [13, 14]. Using carbon nanotubes as an example, the high efficiency of using nanoparticles with a tubular structure in membrane materials has been demonstrated [15–17]. First of all, the interest in carbon nanotubes is caused by their high specific surface area, which leads to the formation of large amounts of nanometer-sized voids and cavities. It has been shown that diffusion and sorption characteristics of carbon nanotubes were superior to those of the known materials [18–20].

The development of easy synthetic methods for non-carbon (most often oxide and oxyhydroxide) tubular structures of various morphologies and surface activities [21] offers possibilities of preparing catalytic and pervaporation composite membranes. It has been shown that morphology of nanotubes, their shape, length and the ratio between internal and external diameters could determine morphological features of a composite [22].

In world practice, the applicability of natural nanomaterials with chrysotile structure in preparation of nanocomposites has been demonstrated [22]. Chrysotile is a lamellar silicate mineral of the serpentine group; its idealized structural formula is $Mg_3Si_2O_5(OH)_4$. According to the modern views, the structural elements of chrysotile are crystalline fibrils in the shape of nanotubes with the average internal diameters of 5 – 7 mm and the average external diameters of 30 – 40 nm. The nanotube (NT) walls are formed by twisting of the double layers due to small mismatch of their diameters (Fig. 1); one of those layers is composed of silicon-oxygen tetrahedrons, and another consists of brucite octahedrons. The thickness of this elementary layer is about 0.75 nm, and the number of layers forming the NT walls usually varies from 20 to 25 [20].

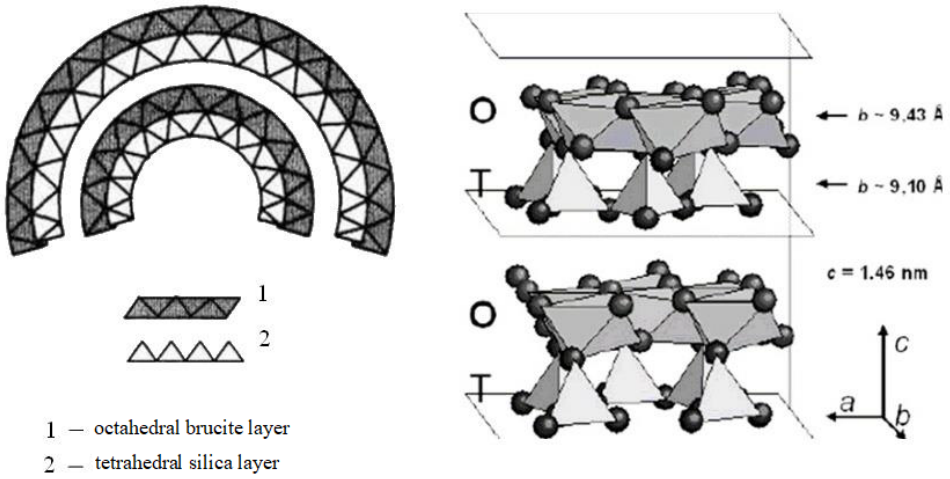

FIG. 1. Structure of chrysotile nanotubes [20]

The transport of liquids and gases through polymer composites containing lamellar nanoparticles with chrysotile structure MMT-15A has been described; the pervaporation nanocomposite membranes containing these chrysotile particles have been prepared [22]. However, the presence of impurities in the natural materials frequently limits the use of natural chrysotile [23]. The use of synthetic nanoparticles with the chrysotile structure made it possible not only to avoid the negative influence of impurities but also to observe a number of specific effects related to the unique structural, morphological, and physical properties of the developed materials.

In this connection, of great interest were the design of new composite materials based on aromatic poly(amide-imide)s filled with inorganic nanotubes of magnesium hydrosilicate $Mg_3Si_2O_5(OH)_4$ (chrysotile) and investigation of the obtained composites (their morphological features, mechanical and transport properties) [22]. The choice of filler material was also caused by the structure of chrysotile nanoparticles, whose surfaces contain polar OH-groups. The methods for controlled hydrothermal synthesis of hydrosilicate NTs were developed and optimized, making it possible to regulate the structure, morphology and size of NTs by varying the synthesis modes and composition of the reaction media [24]. It should be considered that cations of d-elements (Ni, Co, Fe) that partially substitute magnesium in the octahedral layer of the chrysotile structure may change diameter and length of synthetic NTs and affect thermal stability, electric and magnetic characteristics of synthetic substituted hydrosilicates.

The introduction of magnesium-hydrosilicate NTs into polyimide films has been studied earlier; it has been revealed that the presence of this filler resulted in the considerable improvement of mechanical characteristics of the polymer [2,20]. In our earlier works, it has been shown that introduction of hydrosilicate NTs with the chrysotile structure into chemically stable poly(amide-imide) (PAI) led to a new material, the microcomposite whose transport characteristics, thermal stability, and glass transition temperature were significantly higher than those of the initial polymer [25]. This composite consisted of a polymer matrix (poly(diphenyloxide-amide-N-phenylphthalimide)) with NT agglomerates dispersed inside; the size of one such agglomerate approximately corresponded to 10 external diameters of a NT. When a more hydrophilic

polymer (PAI-Ac containing carboxylic groups in diamine fragments of repeating monomer units) was used as a matrix, morphological studies demonstrated more homogeneous distribution of the filler in the matrix; the average amount of NTs in one agglomerate decreased down to 2 – 3 [26].

The studies of transport properties of non-porous films of PAI-based nanocomposites filled with $Mg_3Si_2O_5(OH)_4$ or $Ni_3Si_2O_5(OH)_4$ NTs revealed their increased permeability with respect to polar liquids (water, methanol, ethanol). At the same time, a significant decrease in permeability with respect to weakly polar liquids (toluene, cyclohexane) was observed; in the limiting case, the nanocomposite film even demonstrated barrier properties (very low permeability) [20, 27].

The possibility of modification of transport properties of filled polymer films by variation of their structural and morphological characteristics is widely discussed in scientific literature; these works are reviewed in [20]. Several possible mechanisms of transport of gases and liquids through diffusion membranes of this type were proposed. However, the majority of existing literature data are particular cases and sometimes contradictory observations; they cannot be used to reliably predict transport properties of the developed membranes. One of the problems is the difficulty of analysis of multifactor and multicomponent systems containing low (or very low) amounts of nanosized fillers. The information about the influence of nanoparticles on the properties of nanocomposite membranes is fragmentary, and the factors determining the diffusion transport in these objects are not revealed.

To summarize, the general principles of components combination and regularities of transport of gases and liquids through polymer/NT composites are still poorly understood. It remains unclear what happens to NTs upon immersion into a polymer matrix. The roles of the internal channels of NTs and the external NT/polymer interface in the formation of nanocomposites and the appearance of new mechanical, thermophysical and transport properties have not been explained. To answer these questions, it is necessary to propose an empirical model and to study it using the available physical methods. In this work, the selected model was the PAI-Ac-based nanocomposite containing iron-hydrosilicate NTs with the chrysotile structure. This system was chosen because the hydrothermal synthetic method for morphologically similar NTs containing magnesium, iron, and nickel atoms has been already developed. The nanocomposites on the basis of aromatic PAIs containing magnesium $Mg_3Si_2O_5(OH)_4$ and nickel $Ni_3Si_2O_5(OH)_4$ hydrosilicates with tubular structure have been obtained and investigated earlier. However, the main factor is that the structure of iron-containing nanoparticles can be studied by Mössbauer spectroscopy. To reveal structural features of inorganic nanofillers present in a polymer matrix in low amounts (less than 2 wt.% with respect to polymer mass), it is necessary to use special analytical methods. Mössbauer spectroscopy is a highly sensitive tool for the study of crystalline and amorphous materials; it is absolutely selective to ^{57}Fe isotope and allows one to monitor changes in local environment of iron atoms and to obtain information about phase composition of iron-containing domains. Therefore, it is expected that the use of this method in the studies of correctly chosen model composites will enable one to reveal possible changes in the structure of NTs after their immersion into a polymer matrix.

The aim of the present study is the development of new nanocomposite materials based on aromatic PAI (which was synthesized from diacid chloride of 2-(4-carboxyphenyl)-1,3-dioxoisoindoline-5-carboxylic acid and 3,5-diaminobenzoic acid) filled with iron-containing hydrosilicate NTs.

2. Experimental

2.1. Materials

MgO (“analytical grade”), Fe_2O_3 (“analytical grade”), Fe (“special purity grade”), $SiO_2 \cdot nH_2O$ (silica gel GOST 3056-76), N-methyl-2-pyrrolidone (N-MP) and propylene oxide (Sigma Aldrich, 99 %, CAS 106-89-8) were used without additional purification.

2-(4-carboxyphenyl)-1,3-dioxoisoindoline-5-carboxylic acid was prepared by condensation of trimellitic anhydride ($C_9H_4O_5$) and p-aminobenzoic acid; then the dicarboxylic acid obtained was converted to its diacid chloride by reaction with thionyl chloride as described in [28].

2.2. Polymer synthesis

Synthesis of PAI-Ac (Fig. 2) was performed according to the following protocol [28]. 3.5-Diaminobenzoic acid was dissolved in N-MP containing no more than 0.035 wt.% of moisture at room temperature. Diacid chloride of 2-(4-carboxyphenyl)-1.3-dioxoisoindoline-5-carboxylic acid was added to cooled solution at stirring, then the reaction mixture was left to stand at room temperature for 1.5 h. After cooling the polymer solution and adding propylene oxide, the resulting mixture was stirred at room temperature for 60 min.

PAI-Ac was isolated by precipitation from 10 wt.% polymer solution in N-MP into water. The resulting polymer fibers were filtered, washed with ethanol and dried in oven at 70 °C.

The reduced viscosity of 0.5 wt.% solution of the synthesized PAI-Ac was determined in N-MP at 20 °C and the values of the reduced viscosity η_{red} of two different samples were 1.4 and 1.9 dl/g, which corresponds to molecular masses of 57 and 98 kDa, respectively.

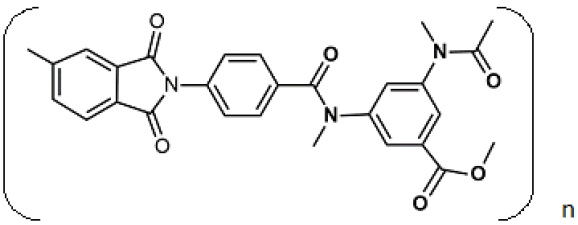

FIG. 2. Chemical structure of PAI-Ac

2.3. Synthesis of nanotubes

Hydrothermal synthesis of $(Mg,Fe_2^+, Fe_3^+)_3Si_2O_5(OH)_4$ hydrosilicate was carried out according to the procedure described in [29].

The specially synthesized $(Mg,Fe)SiO_3$ solid solution containing 25 wt.% FeO was used as an iron-containing starting component. $(Mg,Fe)SiO_3$ was obtained from MgO, Fe_2O_3, Fe, and $SiO_2 \cdot nH_2O$ (silica gel) by solid-phase synthesis performed for 2 – 3 hours in argon atmosphere at a temperature of 1200 °C. Additional component ((Mg,Fe)O) was introduced into the reaction mixture to create the required chrysotile stoichiometry (MgO + FeO) : SiO_2 = 3 : 2. The mixture of $(Mg,Fe)SiO_3$ and (Mg,Fe)O was subjected to hydrothermal treatment in 1/5 – 2 wt.% NaOH solution (400 °C, 70 MPa, 24 h).

2.4. Preparation of samples for studies

2.4.1. Model samples

Preparation of 15 wt.% solution of PAI-Ac polymer in N-MP: N-MP was added to dry polymer and left to stay for 12 hours until the polymer was completely dissolved.

Preparation of nanoparticle suspension: NTs (30 wt.% with respect to the weight of dry polymer) were suspended in N-MP. The suspension was subjected to ultrasound treatment for 1 hour at stirring.

The prepared solution of the PAI-Ac polymer was added to this NT suspension. The concentration of the resulting dispersion (12 wt.% with respect to the weight of dry polymer) was adjusted to 10 wt.% by adding N-MP; after stirring for 20 hours, the dispersion was filtered through a Schott filter.

Model films were prepared by applying a layer of dispersion on a glass plate and removing the solvent during sequential heat treatment at 50 °C for 15 h followed by heating to 150 °C.

2.4.2. Membrane samples

Preparation of 10 wt.% solution of the PAI-Ac polymer in N-MP (5.05 g): 4.55 g of N-MP was added to 0.50 g of dry polymer and left to stay for 12 hours until the polymer was completely dissolved.

Preparation of nanoparticle suspension: nanoparticles (0.0051 g, 1 wt.% with respect to the weight of dry polymer) were suspended in 1.25 g of N-MP. The suspension was subjected to ultrasound treatment for 1 hour at stirring.

The prepared 10 wt.% solution of the PAI-Ac polymer was added to the resulting suspension. The resulting dispersion (NT concentration 8 wt.% with respect to the weight of dry polymer) was stirred for 20 hours, then filtered through a Schott filter. Films were cast onto the surface of glass plates and subjected to heat treatment at 50 °C for 15 h followed by stepwise heating to 150 °C.

2.5. Methods

2.5.1. IR spectroscopy

FTIR spectra were recorded on a Vertex 70 IR-Fourier spectrometer ("Bruker") with a resolution of 4 cm^{-1}, the number of scans was 60. The spectrometer was equipped with a single attenuated total internal reflection (SATR) microattachment ("Pike") with a ZnSe working element. When recording the ATR spectra, a correction was introduced to take into account the penetration depth depending on the wavelength.

2.5.2. ^{1}H NMR spectroscopy

^{1}H NMR spectra were obtained using a Bruker AC-400 spectrometer in deuterated dimethylsulfoxide (DMSO-d_6).

The spectra contain signals at 10.86 ppm and 10.63 ppm that are assigned to NH protons of the amide groups of PAI-Ac.

2.5.3. XRay diffraction analysis

The phase composition of hydrosilicate samples was determined using X-ray diffractometry data (DRON-3M, Cu Kα, Ni filter, $\lambda = 1.54$ Å). Identification of peaks in diffraction patterns was carried out using the PDWin 4.0 software package with a powder diffraction data base based on the ICDD PDF-2 card index.

2.5.4. Electron microscopy

TEM: Transmission electron microscopy studies of NTs were carried out using a JEM 2100-F transmission electron microscope with an accelerating voltage U_{ac} up to 200 kV.

SEM: Film samples were studied with a Supra 55VP scanning electron microscope (ZEISS, Germany) with a secondary electron (SE2) detector. To impart electroconductive properties to the surfaces of tested films and to increase the contrast of obtained images, they were coated with a thin gold layer (15 – 20 nm) by cathode sputtering on a Quorum 150 apparatus (Quorum Technologies Ltd, Laughton, UK).

2.5.5. Mössbauer spectroscopy

Mössbauer spectra of the synthesized samples were recorded on an MS-1-003 electrodynamic spectrometer in the constant acceleration mode with a ^{57}Co (Rh) source at an absorber temperature of 300 K. Isomeric shifts and calibration of the velocity scale were carried out relative to the generally accepted α-Fe standard. Mössbauer spectra were processed in the MOSSFIT program assuming a Lorentzian line shape. The samples were prepared by pressing a certain amount of the tested substance together with a neutral filler (powdered sugar) into tablets about 0.7 mm thick.

2.5.6. Pervaporation experiments

Pervaporation performance of the obtained membranes was tested for different penetrants (sequence → cyclohexane → methanol → ethanol → water or reverse sequence water → ethanol → methanol → cyclohexane) using the autonomous noncontinuous flow laboratory cell, as described in [30] with an operating membrane area of $1.38{\cdot}10^{-3}$ m^2. The process was carried out at constant temperature of 40 °C, at continuous stirring. Permeate vapors were condensed in a receiver using liquid nitrogen. Then the permeate was weighed, and the flux value J (kg·m^{-2}h^{-1}) was calculated using the following equation:

$$J = mS^{-1}t^{-1}, \tag{1}$$

where m is the mass of penetrants permeated through membrane area S in a period t; P (μm·kg·m^{-2}h^{-1}) is the flux (permeation rate) of penetrants normalized to 1 μm membrane thickness.

3. Results and discussion

As discussed in Introduction, immersion of magnesium or nickel-containing nanoparticles of tubular morphology with a chrysotile structure into a polymer matrix can lead to changes in thermophysical and transport properties of a polymer. First of all, this applies to samples belonging to the Mixed Matrix Membranes (MMM) type used in pervaporation. This effect was observed for nanocomposites containing an optimal amount of nanosized inorganic filler; the amount depends on chemical structure of the matrix polymer. This dependence is related to the process of distribution of nanoparticles in the polymer film. In particular, the distribution process is controlled by possible interactions between functional groups present on the surface of nanoparticles and functional groups of the matrix polymer.

When tubular nanoparticles of the general formula $Mg_3Si_2O_5(OH)_4$ synthesized under identical conditions are used as a filler, it is possible to influence the nature of the interaction between inorganic (NT) and organic (polymer) phases. Specifically, we need to select polymers with (or without) functional groups capable of interacting with hydroxyl groups on the outer surface of the NTs. The most significant change in properties (compared to the original polymer) was observed in the case of nanocomposites based on aromatic PAI that was synthesized from 1,3-diaminobenzoic acid. This polymer includes carboxyl-containing fragments in the diamine component of the repeating unit. In polymer-inorganic composites based on this polymer, agglomerates of 1 – 2 NTs are distributed fairly evenly throughout the entire thickness of the film composites. The permeability of composite membranes differs significantly from the permeability of unfilled polymer (Table 1). As shown in Table 1, the PAI-Ac–Mg-NT nanocomposite film is more permeable to both non-polar penetrants (cyclohexane) and polar penetrants (water), but the water permeability increases significantly.

At first glance, the reason for the increase in the permeability of the nanocomposite to water seems obvious, since during its preparation, nanoparticles with hydrophilic groups on the surface are introduced into the polymer matrix. However, a test involving introduction of $Ni_3Si_2O_5(OH)_4$ NTs of a similar structure into PAI under the same conditions showed a slight decrease in water permeability. Consequently, the question of how NTs participate in the preferential mass transfer of water through polymer-inorganic films remains open.

In addition to studying structural and morphological characteristics of the composites, it would be wise to investigate whether the changes occur in the structure of the inorganic dopants themselves after immersion in a polymer matrix. However, this complex problem may be solved only after special additional experiments, possibly involving the preparation of model composites. For this reason, we selected iron-containing NTs of the general formula $Me_3Si_2O_5(OH)_4$

TABLE 1. Pervaporation properties of PAI-Ac-NT in comparison with the base polymer

N	Type of sample	C_{NT}, wt.%	l, μm	T, °C	penetrant	$\boldsymbol{J}$, kg·m^{-2}h^{-1}	P, kg·μm·m^{-2}h^{-1}	P(PAI-Ac-NT)/ P(PAI-Ac)
1	PAI-Ac	—	20	40	water	$6.6 \cdot 10^{-2}$	1.3	—
				20	cyclohexane	$5.0 \cdot 10^{-4}$	$1.0 \cdot 10^{-2}$	—
				40		$9.0 \cdot 10^{-4}$	$1.8 \cdot 10^{-2}$	
2	PAI-Ac – Mg-NT	2	22	40	water	$2.8 \cdot 10^{-1}$	6.2	4.8
				18	cyclohexane	$6.0 \cdot 10^{-4}$	$1.3 \cdot 10^{-2}$	~ 1.3
3	PAI-Ac – Fe-NT	1	15	40	water	$6.1 \cdot 10^{-1}$	9.1	7.0
				40	cyclohexane	$2.3 \cdot 10^{-3}$	$3.4 \cdot 10^{-2}$	1.9

with a chrysotile structure as a filler for preparation of model and membrane composites. This choice was dictated by the possibility of using Mössbauer spectroscopy to study the structure of nanoparticles.

3.1. Inorganic nanoparticles

To form polymer-inorganic composite films, iron-containing hydrosilicate nanoparticles from Mg, Fe-enstatite were synthesized.

According to the XRD data (Fig. 3), the sample is a hydrosilicate with a chrysotile structure.

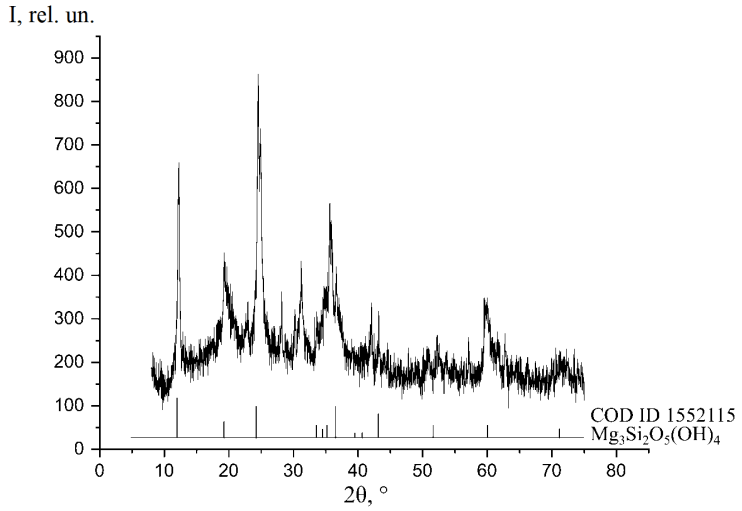

FIG. 3. X-ray diffraction pattern of synthetic $(Mg,Fe)_3Si_2O_5(OH)_4$

Chemical composition of the sample (in mass %): MgO – 31.25, FeO – 9.85, Fe_2O_3 – 5.83, SiO_2 – 40.21 and H_2O – 12.93.

According to the electron microscopy data (Fig. 4), the sample contains cylindrical tubes with a certain amount of "sleeves" type particles with the following geometric dimensions: length 1 – 5 μm, outer diameter 30 – 50 nm, inner diameter 5 – 6 nm.

To investigate crystallinity and chemical structure of the synthesized hydrosilicate NTs, Mössbauer spectroscopy was used. It is known that the Mössbauer spectroscopy, which is a highly sensitive tool for studying crystalline and amorphous materials, has absolute selectivity for the Mössbauer isotope ^{57}Fe. It allows one to obtain valuable information about the coordination position, oxidation state of Fe ions, relative concentration of iron atoms in various states, magnetic structure, etc. [31, 32].

The original synthetic sample of iron-containing chrysotile hydrosilicate NTs from Mg, Fe (enstatite) was studied by the Mössbauer spectroscopy. It should be noted that the results of the Mössbauer research on natural chrysotile were reported in numerous publications [33–35]. From a brief review of publications on the Mössbauer spectroscopy of

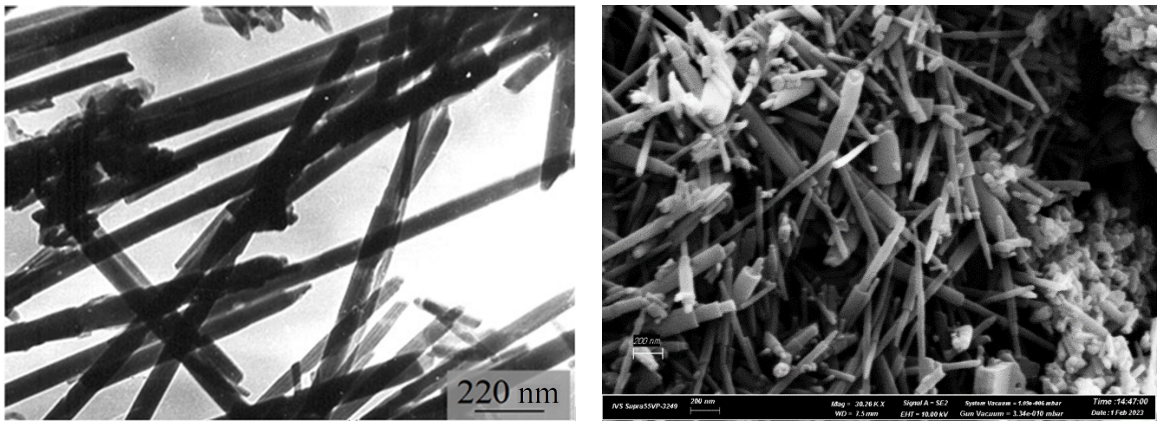

(a) (b)

FIG. 4. (a) TEM images, (b) SEM images of synthesized NT $(Mg,Fe)_3Si_2O_5(OH)_4$

natural chrysotile and the known data on the crystal structure, the following conclusions can be drawn. The Mössbauer spectrum of chrysotile (without Mg impurities) is a superposition of three quadrupole doublets with broadened lines that can be correlated with Fe^{2+} ions replacing Mg positions and Fe^{3+} ions in octahedral and tetrahedral positions of the structure. The Mössbauer study of a synthesized layered hydrosilicate of variable composition with a chrysotile structure was carried out in [36]. It was found that the parameters of the Mössbauer spectrum can only be attributed to the state of Fe^{3+} ions in the octahedral position of the brucite-like layer [37]. In [37], a series of iron-containing chrysotile-asbestos hydrosilicate NTs synthesized from Mg, Fe-enstatite with different amounts of additionally introduced FeO was studied by the Mössbauer spectroscopy in more detail. The degree of oxidation and localization of iron ions by structural positions, the degree of magnetic ordering were revealed. It was shown that Fe in all samples is located predominantly in the paramagnetic phase of the chrysotile structure, and also partially in the magnetic phase of magnetite, whose content decreases with decreasing content of iron introduced into enstatite. One of the samples studied in the above publication (containing 9.8 % FeO and 5.8 % Fe_2O_3) was taken as the initial filler for introduction into the composite polymer composition in this work.

3.2. Preparation and study of nanocomposites

Nanocomposite films containing 1 wt.% of the synthesized Fe-NT were based on the PAI sample that was previously obtained by low-temperature polycondensation. Chemical structure of the polymer is shown in Fig. 2. As described in the Experimental Section, composite films were prepared from dispersions of NTs in PAI solution. These dispersions were applied onto glass plates using a doctor blade. After N-MP was withdrawn in the process of free evaporation, the formed film was mechanically removed from the glass surface. The basic polymer and nanoparticles were selected so as to provide good adhesion between two components of the composite films. Strong interaction occurs between surface hydroxyl groups of the NTs and carboxyl groups of the PAI diamine fragments.

3.2.1. Pervaporation (PV) Properties of MMM

Pervaporation properties of the obtained nanocomposite samples were studied. Although the procedure of sample preparation was generally identical, samples with the same content of nanoparticles exhibited different behavior. Samples of the first type showed high permeability for all studied penetrants and low stability upon exposure to the solvents used in pervaporation experiments. Consider, for example, a sample of the first type with a thickness of 19.3 microns without visible defects and inhomogeneities obtained according to the method described in the Experimental Section. Testing in a pervaporation cell with a dry membrane showed that this sample was defect-free. During pervaporation at 40 °C, the cyclohexane flux through this composite sample was 0.74 $kg{\cdot}m^{-2}h^{-1}$ (flux normalized to the membrane thickness, 14.31 $kg{\cdot}\mu m{\cdot}m^{-2}h^{-1}$), compared to properties of the basic polymer ($1.8 \cdot 10^{-2}$ $kg{\cdot}\mu m{\cdot}m^{-2}h^{-1}$). Thus, introduction of Fe-NT into the PAI-Ac matrix led to the formation of highly permeable samples (of the first type). However, when this nanocomposite membrane was tested in contact with a penetrant after drying, we observed the formation of clearly visible surface cracks and even more serious damage, such as the formation of point defects in the polymer film (due to lack of vacuum when testing a dry membrane in the pervaporation cell).

Samples of the second type showed stability during pervaporation; their transport properties are illustrated in Fig. 5 and Table 1.

MMMs with Fe-NTs (the second type) are characterized by ideal selectivity coefficients α (water/cyclohexane) = 268, α (methanol/cyclohexane) = 191, α (methanol/ethanol) = 5.42 in the first pervaporation rote from cyclohexane to water.

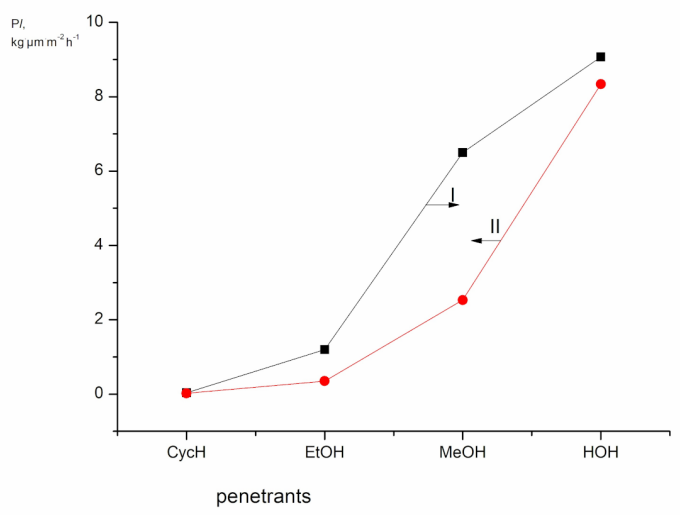

FIG. 5. Pervaporation properties of the MMM membrane containing $(Mg,Fe)_3Si_2O_5(OH)_4$ nanotubes. Flux normalized to membrane thickness [kg·μm·m^{-2}h^{-1}] for penetrants of different polarities when passed through the sample at 40 °C in the following sequences: (I) – cyclohexane (CycH), ethanol (EtOH), methanol (MeOH), water (HOH); (II) – water, methanol, ethanol, cyclohexane

After that, the membrane permeability with respect to polar liquids decreases (in the pervaporation rote from cyclohexane to water), but the cyclohexane permeability of the membrane after this pervaporation cycle remains virtually unchanged.

The permeability of the composite material of the second type exceeds the permeability of the base polymer; this difference is more pronounced than that in the case of magnesium-containing NTs (Table 1). It was assumed that the amounts of surface hydroxyl groups in $Mg_3Si_2O_5(OH)_4$ and $(Mg,Fe)_3Si_2O_5(OH)_4$ tubes are approximately equal. Therefore, we have to discard the idea that an increase in hydrophilicity of the material after its modification determines its permeability.

This pervaporation behavior of composites cannot be explained by irreversible swelling of the membrane in polar liquids either, as evidenced by the data in Fig. 5. The cyclohexane flux normalized to the thickness of the membrane at the beginning of pervaporation is almost equal to that after a full cycle of passing penetrants of different polarities. This also indicates the integrity of the composite film.

It remains unclear why the introduction of Fe-NTs leads to such a significant change in the properties of the polymer. To answer this question, it is necessary to investigate the structure and morphology of the prepared membranes and model composites.

3.2.2. Structural features of polymer and nanocomposite films

3.2.2.1. IR spectroscopy

Using FTIR spectroscopy, the pure PAI-Ac films were compared with nanocomposites of the first type (PAI-Ac films filled with chrysotile).

The FTIR spectrum of pure PAI-Ac contains the bands characteristic of this class of compounds. They are: the band at 3290 cm^{-1}(N-H stretching vibrations of the amide group); bands at 1780 cm^{-1} and 1716 cm^{-1} (symmetric and antisymmetric vibrations of the C=O group of the imide ring); the band at 1659 cm^{-1} (vibrations of the C=O acid group and C=O amide bond); the peak at 1546 cm^{-1} (bending vibrations of the N-H amide bond); and the band at 1367 cm^{-1} (stretching vibrations of the C-N group of the amide ring). In addition, the spectrum exhibits the wide band with a maximum at 3400 cm^{-1} related to the residual solvent (a mixture of amide solvent and water). The peaks assigned to vibrations of OH groups appear near 3400 cm^{-1}.

The important thing to observe here is that the intensity of the broad band with a maximum at 3400 cm^{-1} (vibrations of OH groups) is higher in the spectra of filled films. That is, the OH content in the filled films is higher than that in the PAI-Ac film. An increase in the content of OH groups can occur both due to the presence of hydroxyl groups on the surface of the filler and to more intense sorption of water on the composites (which is probably also related to the filler).

In addition, when the filler is introduced, the band of antisymmetric vibrations of the C=O imide ring at 1716 cm^{-1} shifts to 1719 cm^{-1} and expands into the high-frequency region, which indicates weakening of the hydrogen bonds associated with this band. Further, the intensity of the band at 1367 cm^{-1}, which is attributed to the C-N stretching vibrations of the imide ring, decreases significantly. A change in the system of hydrogen bonds is also indicated by a change in the intensities of the Amide I band (1653 cm^{-1}) and Amide II band (1543 cm^{-1}).

On the other hand, spectral changes in the region of 1716 – 1740 cm^{-1} can be associated with the formation of ester bonds between the COOH groups of the polyacid and OH groups on the surface of the filler. The formation of the

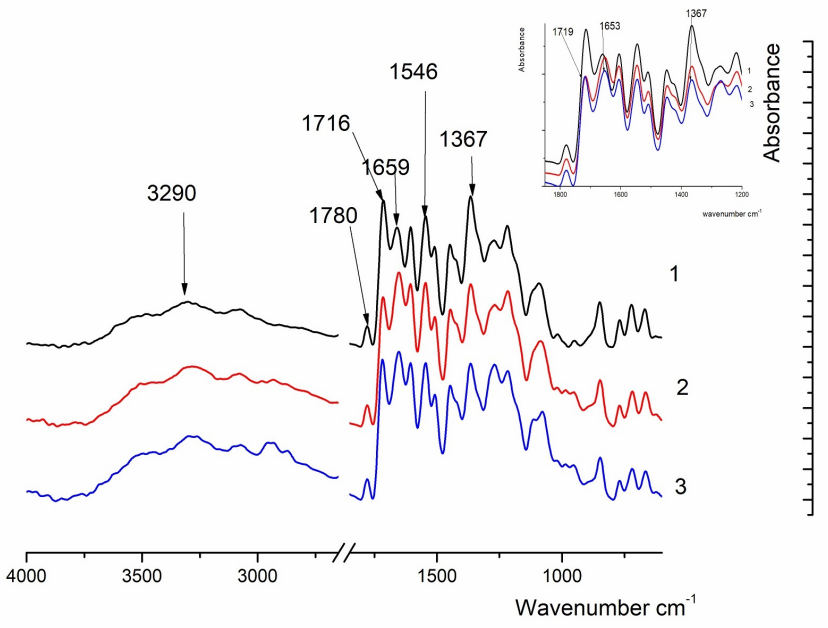

FIG. 6. FTIR spectra of PAI-Ac (1), PAI-Ac–Fe-NT films before pervaporation (2), and PAI-Ac–Fe-NT films after pervaporation (3)

ester bond involving an aromatic acid should lead to the appearance of a new absorption band in the region of 1730 – 1717 cm^{-1}. The appearance of a certain number of ester groups in the system is also accompanied by a change in the system of hydrogen bonds. It should be noted that the esterification reaction is highly likely to occur when a sample is heated above 130 °C, and studied composite films were formed at 150 °C.

However, the formed PAI-Ac based nanocomposite films of the first type (defect-free, judging by the result of a vacuum test on a dry membrane in a pervaporation cell) containing 1 wt.% Fe-NTs showed high permeability to cyclohexane during pervaporation and low stability after direct contact with alcohols (n-ethanol, n-propanol) as penetrants. The films studied during the pervaporation process were re-examined by IR spectroscopy (see above). It was shown that after pervaporation, the shift and broadening of the 1716 cm^{-1} band into the high-frequency region continued. This result indicates gradual weakening of hydrogen bonds involving the C=O groups of the imide ring.

This effect may be related to swelling of the composite film to the point where it loses integrity.

The observed effect in combination with pervaporation properties (see above) absolutely contradicts the results of our previous research (the study of PAI-Ac-based nanocomposite film membranes containing magnesium/nickel hydrosilicate nanoparticles formed under similar conditions). The above works show that the introduction of magnesium or nickel hydrosilicate NTs reduces the permeability of the material to cyclohexane, but significantly increases the permeability to alcohols and water. A consistent explanation for this effect can be provided: the introduced NTs contain hydroxyl groups capable of forming hydrogen bonds. What is the reason of completely different pervaporation behavior exhibited by the Fe-NT-filled composites based on the same PAI-Ac matrix? This is an important question, especially since the used NTs have a similar structure (chrysotile $(Me)_3Si_2O_5(OH)_4$).

Of course, the NTs themselves differed morphologically. While magnesium- or nickel-containing NTs were cylindrical nanoscrolls, then Fe-NTs were cylindrical tubes containing a certain amount of “sleeves” type particles. This difference could lead to differences in the morphology of the composite films.

3.2.2.2. Atomic Force Microscopy (AFM)

Numerous NTs and their fragments located in the near-surface region are observed on the free surface of the film composite (Fig. 7). As seen in Fig. 7, the NTs are uniformly distributed, virtually no aggregates are observed. Taking into account the thickness of polymer coating, the NT thickness was estimated to be $\sim$ 200 nm by the linear profile of the surface area.

The obtained results indicate that the morphology of composites of the first type changes upon contact with cyclohexane, which correlates with the pervaporation data. Although the surface topography practically does not change after swelling in the cyclohexane vapors, the number of NTs observed on the surface increases (due to their ejection from the near-surface region). At the same time, the thickness of the NTs decreases slightly (up to 150 nm) due to the absence of a polymer coating on their surface. It should be noted that the roughness parameters of the matrix surface vary slightly (for a 20 $\times$ 20 micron scanning matrix – R_a = 3.7 nm, R_q = 5.4 nm for the initial composite, R_a = 3.4 nm, R_q = 5.9 nm for the composite after swelling).

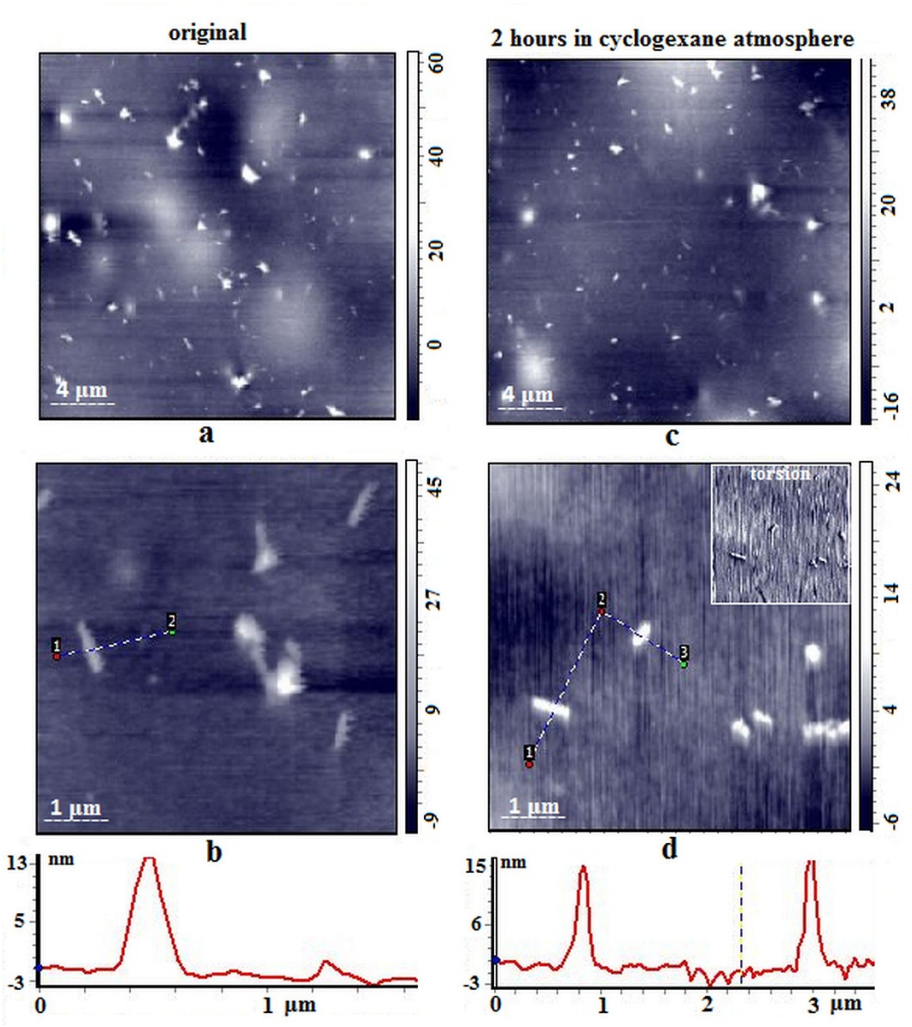

FIG. 7. AFM images of the height of the free surface of the composite: a, b – original; c, d – after 2 hours in cyclohexane atmosphere

Significant changes in the surface topography are visible in the image showing the surface facing the substrate (Fig. 8). The initial surface is characterized by the presence of a large number of cavities; besides, fragments of NTs and their replicas are clearly visible on the surface of the matrix at high magnification. After 2 hours of swelling in cyclohexane vapors, significant morphological changes are observed. Micron-sized aggregates consisting of NT associates and the swollen matrix protrude on the surface, which is seen more clearly in the image taken in the lateral force contrast mode (torsion). At the same time, there are significant changes in the morphology of the fine structure of the sample surface: the surface becomes more friable, nanoporous, the surface roughness increases.

After storage at room temperature for 20 hours, large aggregates of NTs and swollen areas of the matrix are visible over the entire surface of the composite, while the morphology of the matrix changes. The surface is smoothed, the pores are sewn up, the replicas from the fallen NTs are clearly visible.

This tendency of swelling of the film composite with subsequent smoothing of the surface is confirmed by the roughness values. Thus, for the initial film for the 12×12 micron scanning matrix, the values are $R_a = 5.3$ nm, $R_q = 8.1$ nm, after 2 hours of swelling in cyclohexane vapors – $R_a = 30.2$ nm, $R_q = 38.5$ nm, after 20 hours at room temperature $R_a = 12.7$ nm, $R_q = 19.7$ nm.

3.2.2.3. Scanning Electron Microscopy (SEM)

3.2.2.3.1. SEM of MMM. The morphology of cross sections of the nanocomposite film was studied using scanning electron microscopy (Fig. 9) before and after pervaporation.

It was important to reveal structural and morphological properties of the internal layers of the MMM, since the film was formed from the dispersion containing a solvent (N-MP), a polymer (PAI-Ac), and nanoparticles (Fe-NT). NTs were found in the inner layers of the membrane (Fig. 9) and were most clearly seen in the image of the denser film after pervaporation (Fig. 9d,e). It is interesting that the internal structure of the PAI-Ac polymer characteristic of unfilled samples and described in detail by us in [38] is most clearly visible in the samples that passed the pervaporation test.

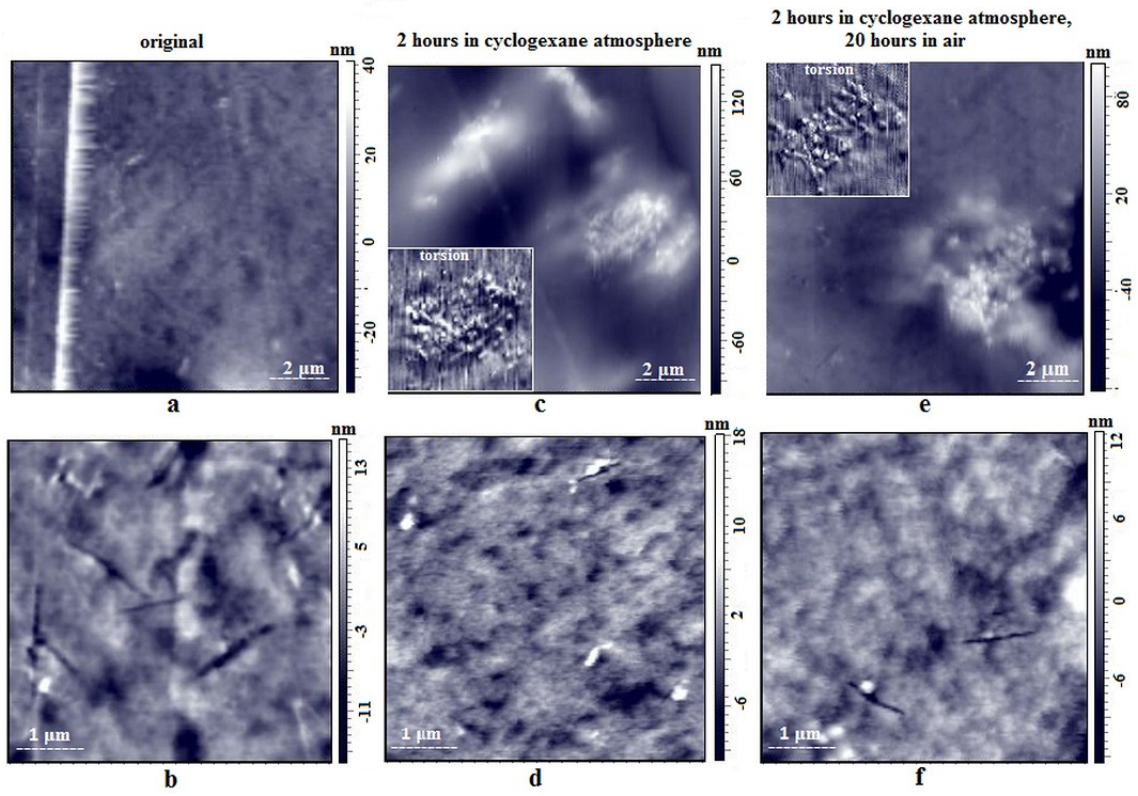

FIG. 8. AFM images of the height of the surface to substrate of the composite: a, b – original; c, d – after 2 hours in cyclohexane atmosphere; e, f – after 2 hours in cyclohexane atmosphere, then 20 hours in air

Apparently, in the case of samples of the first type, the introduction of iron-containing NTs does not cause significant changes in the structural and morphological characteristics of PAI-Ac. However, the formed films are loose and contain cavities, which are larger than those typical of unfilled PAI. After pervaporation and drying, the sample shrinks to form a film of denser morphology. In this case, the NTs come closer together, their concentration in the matrix increases; as a result, they are clearly visible in the inner layers of the membrane (Fig. 9e).

During the pervaporation process and further drying, the film changed its size at least twice, which led to the appearance of pronounced cracks and internal defects. Therefore, it is understandable why after repeated introduction into the pervaporation cell, the membrane failed the vacuum test and was no longer suitable for measurements.

3.2.2.3.2. SEM of the model composite. The question remained as to the state of NTs of this type after immersion in the polymer matrix using the method described in the Experimental Section. To investigate this issue, model composites with a high content of NTs were prepared in the presence of PAI-Ac. This question arose because membranes and model composites were formed by casting dispersions in N-MP; according to the literature data, metal-containing hydrosilicate NTs can change their characteristics in the presence of solvents [39].

As shown in Fig. 10, the polymer covers the entire surface of the sample despite the fact that the inorganic phase (which consists of a set of nanoparticles) predominates in this sample. The NTs coated with a thin layer of polymer are clearly visible in the near-surface region of the sample.

Micrographs of the cross section and internal layers of the sample show that the polymer has penetrated into the sample and formed regions in the interlayer space bordering the inorganic phase. This distribution of the polymer and inorganic phases is confirmed by the data of energy dispersive analysis (EDAS, Table 2) that correspond to the image of the surface of the inner layer of the model film at a magnification of 2000 (Fig. 11). It can be seen that in the regions corresponding to spectra 1, 2, 3, 4, the average concentration of nanoparticles is low (silicon concentration 2.2 – 2.8 wt.%), and in the "point" regions corresponding to spectra 5, 6, 7, nanoparticles are localized. Spectrum 8 shows the presence of voids in the interlayer space of the sample.

Thus, in this model composite, the concentration of nanoparticles is so high that it is possible to study them in a limited time using the Mössbauer method, while the concentration of the polymer and its distribution allow one to trace its influence on the state of the inorganic phase. Recall that the model composites were obtained by the same method and under the same conditions as the membranes (casting from dispersions in N-MP).

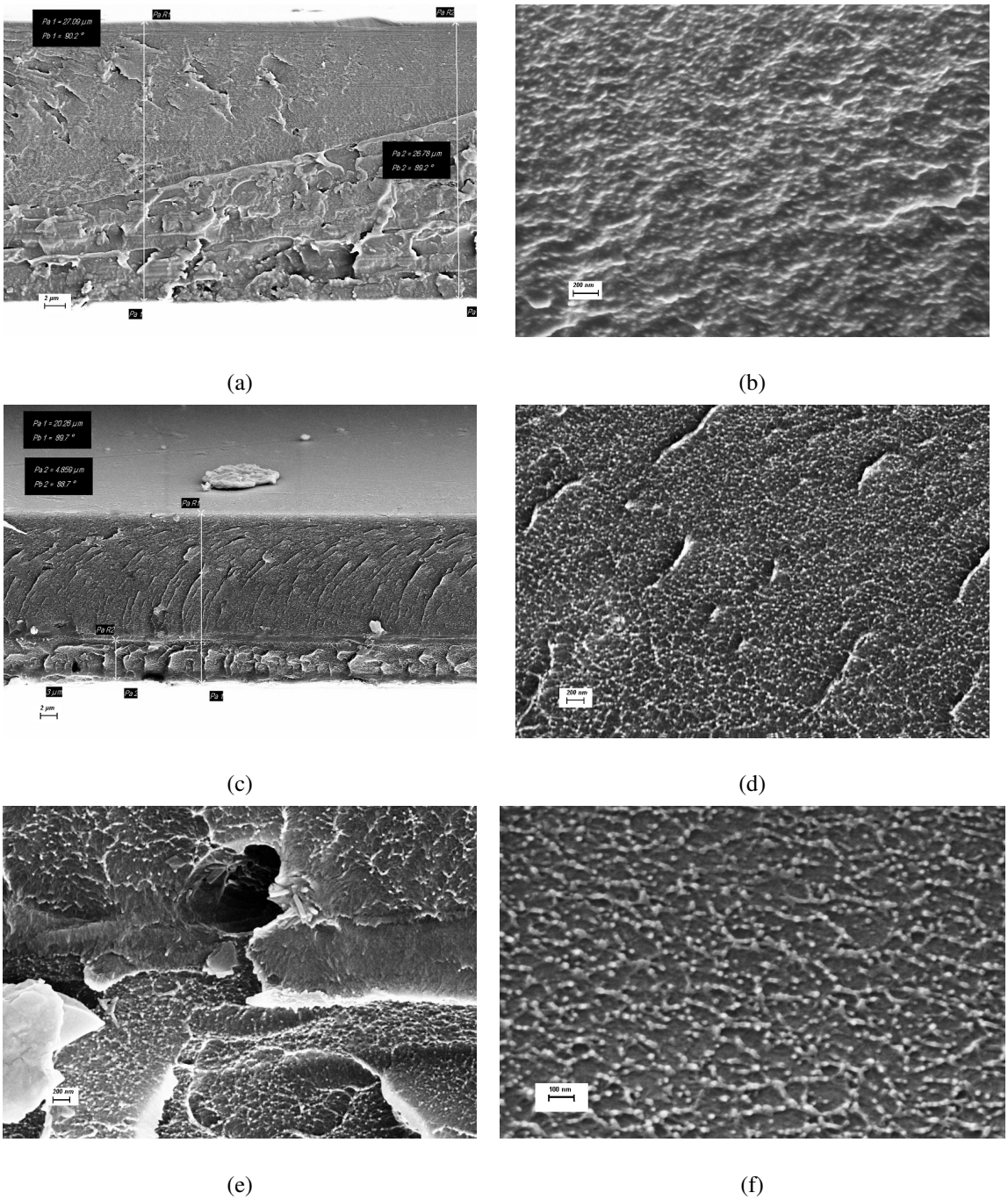

FIG. 9. SEM-images of the cross section (a – e) and internal layers (b,d,e) of a 27 μm thick MMM sample before (a,b) and after (c – e) pervaporation; SEM – image of the cross section of the PAI-Ac film (f)

It is interesting that the nature of the internal structure of the model films (Fig. 10f) is dictated by the polymer matrix, and their structural and morphological features are similar to the structure of the PAI-Ac films [38], as well as the MMM-film presented in Fig. 9.

3.2.2.4. Mössbauer spectroscopy

We attempted to use Mössbauer spectroscopy to analyze structural features of NTs immersed in a polymer matrix.

Figure 12 shows the Mössbauer spectra of chrysotile hydrosilicate NTs (original sample) and nanotubes included in the composite film (PAI-K + MgFe chrysotile NTs).

The results of the mathematical decomposition into individual subspectra of these samples are presented in Table 3. The data presented above show that the Fe ions in the samples exist in the magnetic (magnetite) and paramagnetic (chrysotile) phases. The areas under the Mössbauer absorption lines were used to calculate the distribution of total iron

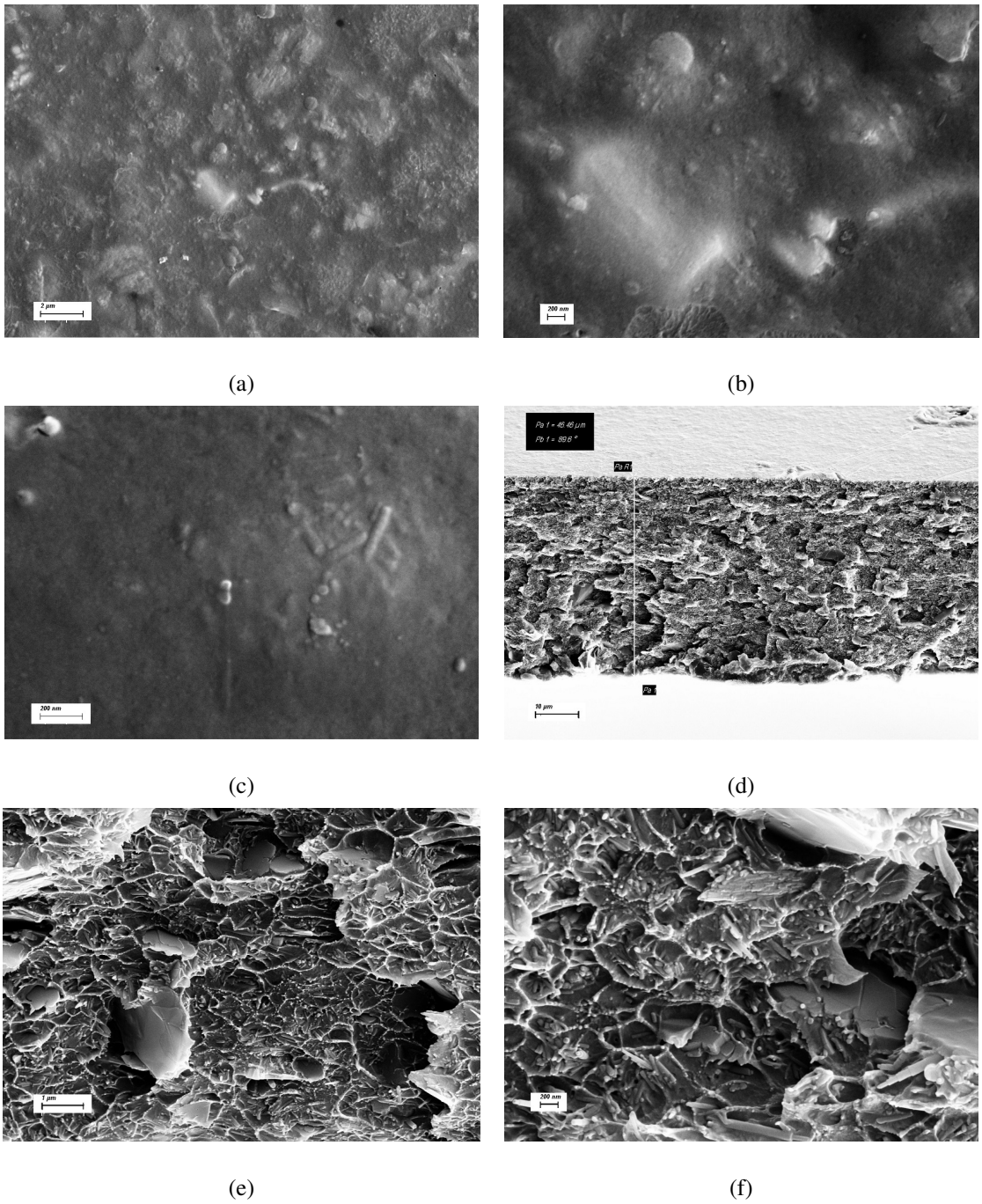

FIG. 10. SEM images of the model sample: (a, b, c) surface fragments, (d) cross-section, (e, f) internal layers

between the Fe^{2+} and Fe^{3+} states and the ratio of iron amounts in magnetite and chrysotile NTs (~ 1 in the original sample, 1.29 in the composite). It is known that magnetite is a mixed-valence system and crystallizes into an inverted spinel structure at room temperature. This structure contains tetrahedral positions with Fe^{3+} cations and octahedral positions with an equal number of randomly distributed Fe^{3+} and Fe^{2+} cations. As a result of rapid electron exchange between iron ions of different valences in the octahedral position, an intermediate electronic state with an average value of the isomer shift parameter appears. The Mössbauer spectroscopy allows one to qualitatively distinguish the distribution of Fe^{2+} and Fe^{3+} ions between tetrahedral and octahedral positions in magnetite based on the characteristic Heff values (see Table 3).

The paramagnetic part of the spectrum of the initial sample consists of two doublets, which, according to the typical IS and QS values (Table 3), can be attributed to Fe ions of different valences in the tetrahedral and octahedral ($Fe^{3+}{}_{tetr}$ and $Fe^{2+}{}_{oct}$) positions of the chrysotile structure. Fe^{2+} and Mg^{2+} ions are isomorphic; therefore, Fe^{2+} replaces Mg in the brucite (outer) layer of the chrysotile NT. It should be noted that inclusion of Fe^{3+} in the octahedral position was not detected in the original sample, in contrast to the spectra of natural chrysotiles of various origins, as well as those of the synthetic layered hydrosilicate of variable composition with a chrysotile structure [36]. Obviously, under the synthetic

TABLE 2. Elemental EDAS analysis (normalized; concentrations in mass %) of the surface of the inner layer of the sample in accordance with Fig. 11

Spectrum	C	N	O	Na	Mg	Si	Cl	Fe	Total
1	60.97	8.39	22.45	0.56	2.82	2.40	0.75	1.65	100.00
2	59.96	5.24	20.56	2.28	2.35	2.73	3.89	2.99	100.00
3	61.06	6.73	23.86	0.32	3.32	2.77	0.22	1.72	100.00
4	62.12	8.40	22.75	0.24	2.72	2.23	0.08	1.47	100.00
5	75.19	0.00	16.54	0.35	3.59	4.33	0.00	0.00	100.00
6	38.52	0.00	39.67	0.52	8.66	6.29	0.00	6.35	100.00
7	55.18	0.00	28.84	0.32	7.42	6.17	0.06	2.02	100.00
8	69.69	0.00	25.25	0.17	2.30	1.80	0.00	0.79	100.00
Average	60.34	3.60	24.99	0.60	4.15	3.59	0.62	2.12	100.00
Std. deviation	10.79	3.97	6.91	0.69	2.46	1.79	1.35	1.92	

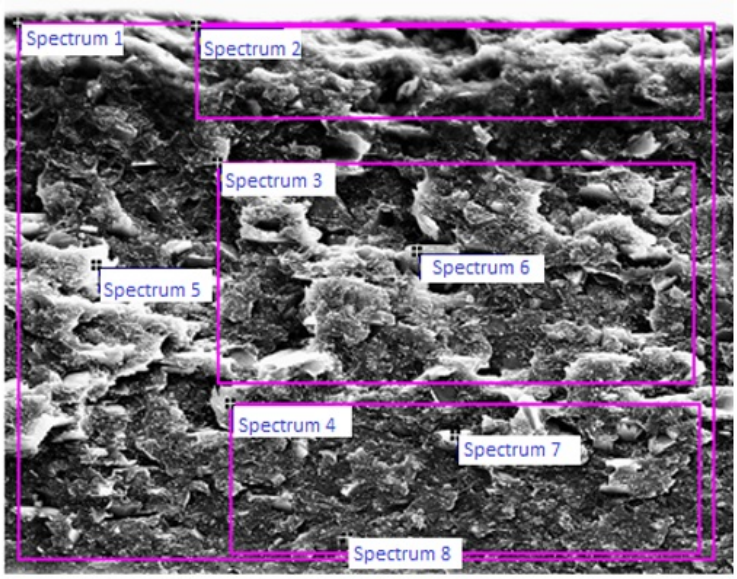

FIG. 11. SEM image of the surface of the inner layer of the model sample at a magnification of $\times 2000$

conditions for the initial sample, Fe^{3+} only enters into the tetrahedral position. Thus, the possibility exists of targeted synthesis of samples with predetermined properties.

The Mössbauer parameters in the sample of chrysotile NTs included in composite films underwent minor changes. Mössbauer parameters (IS, QS, Heff) remained the same within the measurement error. A slight increase in the error in the calculated values of the Mössbauer parameters $Fe^{2+}{}_{oct}$ in the composite sample is correlated with a decrease in the overall magnitude of the Mossbauer resonance absorption effect, which may be associated with the preparation conditions of this film composite. The Fe^{3+}/Fe^{2+} ratio in the paramagnetic part of the sample in the polymer film decreased to 4.4 compared to the original sample (5.2), mainly due to a change in the relative fraction of magnetite.

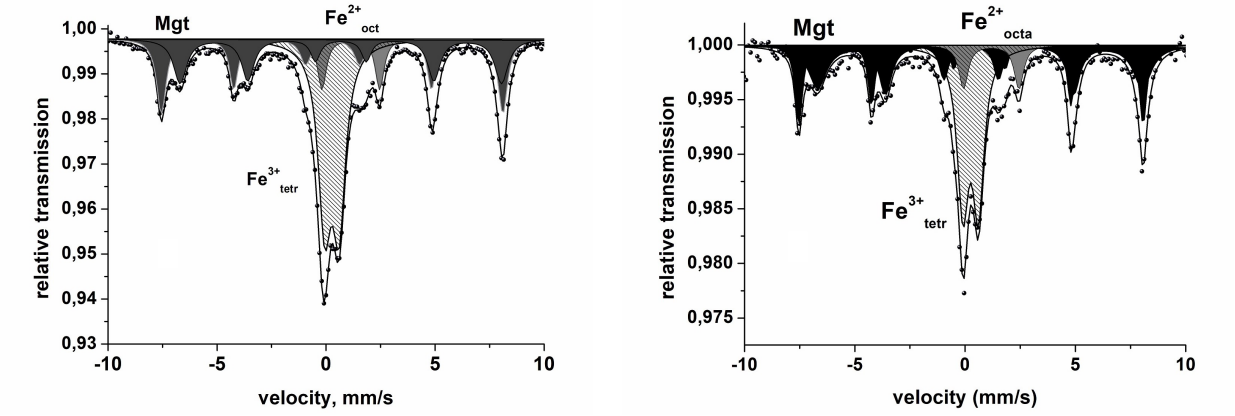

(a) (b)

FIG. 12. Mössbauer spectra of chrysotile hydrosilicate nanotubes: a – original sample; b – nanotubes in the composite

TABLE 3. Mössbauer effect parameters of the samples (a – original sample; b – nanotubes in the composite) at 300 K

Sample	Spectral component	IS, mm/s	QS, mm/s	S, %	Heff, T
a	Fe^{3+} tetr	0.27 ± 0.01	0.66 ± 0.01	41.56	—
	Fe^{2+} oct	1.14 ± 0.02	2.65 ± 0.04	8.05	—
	Fe^{3+} tetr	0.29 ± 0.01	0.02 ± 0.02	26.13	48.64 ± 0.09
	Mgt				
	(Fe^{2+}+Fe^{3+}) oct	0.68 ± 0.02	0.01 ± 0.02	24.25	45.77 ± 0.18
b	Fe^{3+} tetr	0.25 ± 0.04	0.70 ± 0.08	35.57	—
	Fe^{2+} oct	1.18 ± 0.12	2.51 ± 0.25	8.08	—
	Fe^{3+} tetr	0.27 ± 0.01	0.01 ± 0.02	25.87	48.49 ± 0.11
	Mgt				
	(Fe^{2+} +Fe^{3+}) oct	0.66 ± 0.03	-0.02 ± 0.06	30.48	45.74 ± 0.29

Note: IS – isomer shift (Isomer shift); QS – quadrupole splitting, (Quadrupole splitting); S – relative fraction of iron atoms in a particular position; Heff – ultrafine magnetic field, tesla (Hyperfine field, T)

4. Conclusions

Introduction of hydrosilicate NTs $(Mg,Fe)_3Si_2O_5(OH)_4$ with a chrysotile structure into the PAI-Ac polymer matrix leads to the formation of two types of composite membranes, depending on the molecular weight of PAI. When the polymer with relatively low molecular weight is used, the so-called "composite films of the first type" are formed. They are not stable during pervaporation that involves contact with organic penetrants such as cyclohexane and ethanol. Membranes of this type exhibit high permeability to cyclohexane compared to the base polymer. However, they swell significantly during pervaporation and cannot be reused, because defects appear in films after drying. Membranes of the "second type" prepared of the polymer with higher molecular weight are stable during pervaporation. Besides, they are more permeable to polar liquids (compared to the base polymer and MMMs containing $Mg_3Si_2O_5(OH)_4$ NTs). Thus, the introduction of iron-containing NTs into PAI-Ac leads to an increase in the permeability of MMM. The results obtained correlate

with the structural characteristics of the membranes. The introduction of NTs into the polymer does not cause significant changes in the structural characteristics of the nanoparticles. However, a slight increase in the amount of magnetite in NTs indicates that some part of NTs are destructed in the process of formation of the "first type composites".

The properties of the obtained MMMs deserve further study; a possible line of investigation is introduction of iron-containing nanoparticles of other structure and morphology into the PAI-Ac polymer matrix.

References

[1] Sreekumar T.V., Liu T., Min B.G., Guo H., Kumar S., Hauge R.H., Smalley R.E. Polyacrylonitrile Single-Walled Carbon Nanotube Composite Fibers. *Adv. Mat.*, 2004, **16** (1), 58.

[2] Yudin V.E., Otaigbe J.U., Gladchenko S., Olson B.G., Nazarenko S., Korytkova E.N., Gusarov V.V. New polyimide nanocomposites based on silicate type nanotubes: Dispersion, processing and properties. *Polymer*, 2007, **48**, P. 1306–1315.

[3] Zhen-Liang X.U., Li-Yun Y.U., Ling-Feng H.A.N. Polymer-nanoinorganic particles composite membranes: a brief overview. *Front. Chem. Eng. China*, 2009, **3** (3), 318.

[4] Samad A., Lau K.Y., Khan I.A., Khoja A.H., Jaffar M.M., Tahir M. Structure and breakdown property relationship of polyethylene nanocomposites containing laboratory-synthesized alumina, magnesia and magnesium aluminate nanofillers. *J. Phys. Chem. Solids*, 2018, **120**, P. 140–146.

[5] Li S., Lin M.M., Toprak M.S., Kim D.K., Muhammed M. Nanocomposites of polymer and inorganic nanoparticles for optical and magnetic applications. *Nano Reviews*, 2010, **1**, 5214.

[6] Jeon I-Y., Baek J-B. Nanocomposites Derived from Polymers and Inorganic Nanoparticles. *Materials*, 2010, **3** (6), 3654.

[7] Sawunyama L., Ajiboye T.O., Oyewo O., Onwudiwe D.C. Ceramic-polymer composite membranes: Synthesis methods and environmental applications. *Ceramics Int.*, 2024, **50**, P. 5067–5079.

[8] Vu De Q., Koros W. J., Miller S. J. High Pressure CO2/CH4 Separation Using Carbon Molecular Sieve Hollow Fiber Membranes. *Industrial & engineering chemistry research* 2002, **41** (3), 367.

[9] Mahajan R., Koros W.J., Thundyil M. Mixed matrix membranes: important and challenging. *Membrane Technology*, 1999, **105**, 6.

[10] Moaddeb M., Koros W.J. Occlusion of pores of polymeric membranes with colloidal silica. *J. Membrane Sci.*, 1997, **136** (1), P. 273–277.

[11] Koros W.J., Coleman M.R., Walker D.R.B. Controlled permeability polymer membranes. *Annu. Rev. Mater. Sci.*, 1992, **22**, P. 47–89.

[12] Singh-Ghosal A., Koros W.J. Energetic and entropic contributions to mobility selectivity in glassy polymers for gas separation membranes. *Ind. Eng. Chem. Res.*, 1999, **38**, 3647.

[13] Pinnau I., He Z.J., Morisato A. Nanostructured poly (4-methyl-2-pentyne)/silica hybrid membranes for gas separation. *Abstr. Pap. Am. Chem. Soc. Part 2*, 2001, **222**, U368.

[14] Nunes S.P., Peinemann K.V., Ohlrogge K., Alpers A., Keller M., Pires A.T.N. Membranes of poly(ether imide) and nanodispersed silica. *J. Membrane Sci.*, 1999, **157**, 219.

[15] Potschke P., Fornes T.D., Paul D.R. Rheological behavior of multiwalled carbon nanotube/polycarbonate composites. *Polymer*, 2000, **41**, 3861.

[16] Baughman R.H., Zakhidov A.A., Heer W.A. Carbon Nanotubes – the Route Toward Applications. *Science*, 2002, **297** (5582), 787.

[17] Sholl D.S., Johnson J.K. Making High-Flux Membranes with Carbon Nanotubes. *Science*, 2006, **312** (5776), P. 1003–1004.

[18] McGinnis R.L., Reimund K., Ren J., Xia L., Chowdhury M.R., Sun X., Abril M., Moon J.D., Merrick M.M., Park J., Stevens K.A., McCutcheon J.R., Freeman B.D. Large-scale polymeric carbon nanotube membranes with sub–1.27 nm pores. *Sci. Adv.*, 2018, **4** (3), 1700938.

[19] Geise G.M., Paul D.R., Freeman B.D. Fundamental water and salt transport properties of polymeric materials. *Progress in Polymer Science*, 2014, **39** (1), P. 1–42.

[20] Kononova S.V., Gubanova G.N., Korytkova E.N., Sapegin D.A., Setnickova K., Petrychkovych R., Uchytil P. Polymer Nanocomposite Membranes. *Appl. Sci.*, 2018, **8**, 1181.

[21] Korytkova E.N., Maslov A.V., Pivovarova L.N., Drozdova I.A., Gusarov V.V. Formation of $Mg_3Si_2O_5(OH)_4$ nanotubes under hydrothermal conditions. *Glass Phys. Chem. (Engl. Transl.)*, 2004, **30** (1), P. 51–55.

[22] Kononova S.V., Korytkova E.N., Romashkova K.A., Kuznetsov Y.P., Gofman I.V., Svetlichnyi V.M., Gusarov V.V. Nanocomposite based on polyamidoimide with hydrosilicate nanoparticles of varied morphology. *Russian J. of Applied Chemistry*, 2007 **80** (12), P. 2142–2148.

[23] Skuland T., Maslennikova T., Lag M., Gatina E., Serebryakova M., Trulioff A., Kudryavtsev I., Klebnikova N., Kruchinina I., Schwarze P. E., Refsnes M. Synthetic hydrosilicate nanotubes induce low pro?inflammatory and cytotoxic responses compared to natural chrysotile in lung cell cultures. *Basic & Clinical Pharmacology & Toxicology*, 2019, *126* (2), 13341.

[24] Korytkova E.N., Pivovarova L.N., Drozdova I.A., Gusarov V.V. Synthesis of nanotubular nickel hydrosilicates and nickel-magnesium hydrosilicates under hydrothermal conditions. *Glass Physics and Chemistry*, 2005, **31** (6), P. 797–802.

[25] Gubanova G.N., Kononova S.V., Vylegzhanina M.E., Sukhanova T.E., Grigor'Ev A.I., Romashkova K.A., Svetlichnyi V.M., Korytkova E.N., Christi M., Timpu D., Harabagiu V. Structure, morphology, and thermal properties of nanocomposites based on polyamidoimides and hydrosilicate nanotubes. *Russian J. of Applied Chemistry*, 2010, **83** (12), P. 2175–2181.

[26] Kononova S.V., Korytkova E.N., Maslennikova T.P., Romashkova K.A., Kruchinina E.V., Potokin I.L., Gusarov V.V. Polymer-inorganic nanocomposites based on aromatic polyamidoimides effective in the processes of liquids separation. *Russ. J. Gen. Chem.*, 2010, **80**, 1136.

[27] Gubanova G.N., Sukhanova T.E., Vylegzhanina M.E., Lavrentiev V.K., Romashkova K.A., Kutin A.A., Maslennikova T.P., Kononova S.V. Analysis of the surface morphology, structure and properties of polyamidoimide nanocomposites with tubular hydrosilicates. *J. of Surf. Invest.: X-ray, Synchrotron and Neutron Techniques*, 2017, **11** (5), 1022.

[28] Gusinskaya V.A., Koton M.M., Batrakova T.V., Romashkova K.A. Poly(amino) imides based on symmetrical and asymmetrical imido acid dichlorides. *Polymer Science U.S.S.R.*, 1976, **A18** (12), P. 3062–3068.

[29] Korytkova E.N., Pivovarova L.N., Semenova O.E., Drozdova I.A., Povinich V.F., Gusarov V.V. Hydrothermal synthesis of nanotubulal Mg-Fe hydrosilicate. *Russian J. of Inorganic Chemistry*, 2007, **52** (3), P. 338–344.

[30] Kononova S.V., Kremnev R.V., Suvorova E.I., Baklagina Y.G., Volchek B.Z., Uchytil P., Shabsels B.M., Romashkova K.A., Setnickova K., Reznickova J. Pervaporation membranes with poly(γ-benzyl-l-glutamate) selective layers for separation of toluene–n-heptane mixtures. *J. Membr. Sci.*, 2015, **477**, 14.

[31] Eckhard Bill, in ^{57}*Fe-Mössbauer Spectroscopy and Basic Interpretation of Mössbauer Parameters*, (Eds: Crichton R.R., Louro R.O.), Elsevier, 2013, **5**, P. 109–130.

[32] Eckhard Bill, in ^{57}*Fe-Mössbauer spectroscopy and basic interpretation of Mössbauer parameters*, (Eds: Crichton R.R., Louro R.O.), Elsevier, 2020, **6**, P. 201–228.

[33] Boulatov F.M., Ivoilova E.Kh. Structural features of chrysotile asbestos according to Mössbauer spectroscopy data. *Mineralogical J.*, 1985, **7** (2), P. 22–29.
[34] Ristić M., Czakó-Nagy I., Musić S., Vértes A. Spectroscopic characterization of chrysotile asbestos from different regions. *J. of Molec. Struct.*, 2011, **993**, 120.
[35] Lemos B.R.S., Teixeira A.P.C., Ardisson J.D., Macedo W.A.A., Fernandes-Outon L.E., Amorim C.C., Moura F.C.C., Lago R.M. Magnetic Amphiphilic Composites Applied for the Treatment of Biodiesel Wastewaters. *Appl. Sci.*, 2012, **2** (2), 513.
[36] Krasilin A.A., Panchuk V.V., Semenov V.G., Gusarov V.V. Formation of variable-composition iron(III) hydrosilicates with the chrysotile structure. *J. of Gen. Chem.*, 2016, **86** (12), 1943.
[37] Kozlov V.S., Maslennikova T.P., Korytkova E.N., Kononova S.V. Möessbauer study of iron ions localization in the structure of synthetic chrysotile-asbestos hydrosilicate nanotubes. *Neutron Scattering in Condensed Matter Research (RNICS-2021)*, Russia, Ekaterinburg, 2021, **306**.
[38] Gubanova G.N., Timpu D., Cristea M., Kononova S.V., Korytkova E.N., Sapegin D.A., Saprykina N.N., Volkov A.Y., Klechkovskaya V.V. Nanocomposites Based on Poly(Amide-Imide) Matrix with Na–Mg Triple Chain Hydrosilicate. *Crystallography Reports*, 2021, **66** (7), 1185.
[39] Kryazheva K.S., Korytkova E.N., Maslennikova T.P., Ugolkov V.L. Interacton of chrisotyl nanotubes with water-alcohol solutons at different temperature-time parameters. *Glass Phys. Chem.*, 2012, **38** (1), 122.

Submitted 2 April 2024; revised 5 April 2024; accepted 6 April 2024

Information about the authors:

Svetlana V. Kononova – Institute of Macromolecular Compounds Russian Academy of Science, 199004, Bolshoy pr. 31, St. Petersburg, Russia; ORCID 0000-0001-5468-3909; svetlanavkononova@gmail.com

Galina K. Lebedeva – Institute of Macromolecular Compounds Russian Academy of Science, 199004, Bolshoy pr. 31, St. Petersburg, Russia; ORCID 0000-00002-2384-1422; constanta2011.lebedeva@mail.ru

Valery S. Kozlov – Petersburg Nuclear Physics Institute named by B. P. Konstantinov of National Research Centre "Kurchatov Institute", Gatchina, Russia; kozlov_vs1@pnpi.nrcki.ru

Eleonora N. Korytkova – Russian Academy of Science, Grebenshchikov Institute of Silicate Chemistry, St. Petersburg, Russia; elkor@list.ru

Tatyana P. Maslennikova – Russian Academy of Science, Grebenshchikov Institute of Silicate Chemistry, St. Petersburg, Russia; ORCID 0000-0001-9459-8960; sveta_k@hq.macro.ru

Elena V. Kruchinina – Institute of Macromolecular Compounds Russian Academy of Science, 199004, Bolshoy pr. 31, St. Petersburg, Russia; ORCID 0000-0002-3628-0863; evkruchinina@mail.ru

Elena N. Vlasova – Institute of Macromolecular Compounds Russian Academy of Science, 199004, Bolshoy pr. 31, St. Petersburg, Russia; ORCID 0000-0002-4644-0445; spectra@imc.macro.ru

Natalia N. Saprykina – Institute of Macromolecular Compounds Russian Academy of Science, 199004, Bolshoy pr. 31, St. Petersburg, Russia; ORCID 0000-0002-9240-1690; nataly-saprykina@yandex.ru

Galina N. Gubanova – Institute of Macromolecular Compounds Russian Academy of Science, 199004, Bolshoy pr. 31, St. Petersburg, Russia; ORCID 0000-0003–548-9976; gubanovagn@yandex.ru

Milana E. Vylegzhanina – Institute of Macromolecular Compounds Russian Academy of Science, 199004, Bolshoy pr. 31, St. Petersburg, Russia; ORCID 0000-0002-5468-7595; v.e.milana@gmail.com

Vasiliy T. Lebedev – Petersburg Nuclear Physics Institute named by B. P. Konstantinov of National Research Centre "Kurchatov Institute", Gatchina, Russia; ORCID 0000-0003-4894-0862; lebedev_vt@pnpi.nrcki.ru

Conflict of interest: the authors declare no conflict of interest.